JNeurosci
THE JOURNAL OF NEUROSCIENCE

Research Articles: Systems/Circuits

THE BASOLATERAL AMYGDALA SENDS A MIXED (GABAERGIC AND GLUTAMATERGIC) PROJECTION TO THE MEDIODORSAL THALAMIC NUCLEUS

https://doi.org/10.1523/JNEUROSCI.1924-22.2022

Cite as: J. Neurosci 2023; 10.1523/JNEUROSCI.1924-22.2022

Received: 11 October 2022
Revised: 13 December 2022
Accepted: 20 December 2022

THE BASOLATERAL AMYGDALA SENDS A MIXED (GABAERGIC AND GLUTAMATERGIC) PROJECTION TO THE MEDIODORSAL THALAMIC NUCLEUS

Nowrin Ahmed and Denis Pare*

Center for Molecular and Behavioral Neuroscience,
Rutgers University, Newark, NJ 07102.

Abbreviated title: Amygdala projection to the mediodorsal thalamus

Correspondence should be sent to:
Denis Paré
Center for Molecular & Behavioral Neuroscience
Rutgers University-Newark
197 University Avenue, Newark, NJ 07102
Phone: (973) 353-3251
Email: pare@rutgers.edu

This paper contains 8 figures and 4 tables. 27 text pages.

Word counts: Abstract, 250; Introduction, 528; Discussion, 1193.

Acknowledgements:
This work was supported by R01 grant MH-107239 to DP from NIMH. NA was supported by the Behavioral and Neural Sciences Graduate Program of Rutgers University.

Conflict of interest:
The authors declare that they have no competing financial interests.

Author contributions:
NA and DP conceived the experimental design. NA carried out the tracing, immunohistochemical and electrophysiological experiments. NA and DP analyzed the data. DP made the figures. DP wrote the first draft of the manuscript. Both authors contributed to refine the manuscript.

ABSTRACT

The medial prefrontal cortex (mPFC) receives converging inputs from the mediodorsal thalamic nucleus (MD) and basolateral amygdala (BLA). Although many studies reported that the BLA also projects to MD, there is conflicting evidence regarding this projection, with some data suggesting that it originates from GABAergic or glutamatergic neurons. Therefore, the present study aimed to determine the neurotransmitter used by MD-projecting BLA cells in male and female rats. We first examined whether BLA cells retrogradely labeled by Fast Blue infusions in MD are immunopositive for multiple established markers of BLA interneurons. A minority of MD-projecting BLA cells expressed somatostatin (~22%) or calretinin (~11%) but not other interneuronal markers, suggesting that BLA neurons projecting to MD not only include glutamatergic cells, but also long-range GABAergic neurons. Second, we examined the responses of MD cells to optogenetic activation of BLA axons using whole-cell recordings *in vitro*. Consistent with our immunohistochemical findings, among responsive MD cells, light stimuli typically elicited isolated EPSPs (73%) or IPSPs (27%) as well as coincident EPSPs and IPSPs (11%). Indicating that these IPSPs were monosynaptic, light-evoked EPSPs and IPSPs had the same latency and the IPSPs persisted in the presence of ionotropic glutamate receptor antagonists. Overall, our results indicate that the BLA sends a mixed, glutamatergic-GABAergic projection to MD, which likely influences coordination of activity between BLA, MD, and mPFC. An important challenge for future studies will be to examine the connections formed by MD-projecting glutamatergic and GABAergic BLA cells with each other and other populations of BLA cells.

SIGNIFICANCE STATEMENT

The mediodorsal thalamic nucleus (MD) and basolateral amygdala (BLA) send convergent projections to the medial prefrontal cortex (mPFC). Although many studies reported that the BLA also projects to MD, there is conflicting evidence as to whether this projection is glutamatergic or GABAergic. By combining tract tracing, immunohistochemistry, optogenetics, and patch clamp recordings in vitro, we found that BLA neurons projecting to MD not only include glutamatergic cells, but also long-range GABAergic neurons. Differential recruitment of these two contingents of cells likely influences coordination of activity between the BLA, MD, and mPFC.

INTRODUCTION

Although the basolateral complex of the amygdala (BLA) is often likened to the cerebral cortex (Carlsen and Heimer, 1988), some of its features are inconsistent with this analogy. Reminiscent of cortex, the BLA contains a similar complement of cell types, including a majority of spiny glutamatergic projection cells and a heterogeneous group of aspiny inhibitory interneurons (McDonald, 1992; Smith and Paré, 1994; Mascagni and McDonald, 2007; Spampanato et al., 2011; Capogna, 2014; Vereczki et al., 2021). Also, as in cortex where inter-related areas tend to project to the same striatal territories (Alexander et al., 1986), the BLA innervates cortical areas that target the same regions of the striatum as it does (Groenewegen et al., 1990; McDonald, 1991).

However, the analogy breaks down when considering BLA's thalamic connections. Unlike the generally reciprocal connections between the dorsal thalamus and cortex (Jones, 2007), most dorsal thalamic nuclei projecting to the BLA receive little or no return afferents. Indeed, the BLA receives heavy inputs from parts of the ventroposterior and medial geniculate nuclei as well as multiple thalamic nuclei located near the midline, most of which do not receive significant projections from the BLA (Krettek and Price, 1977; Ottersen and Ben-Ari, 1979; LeDoux et al., 1990; Su and Bentivoglio, 1990; Turner and Herkenham, 1991; Vertes et al., 2015).

The best documented BLA projection to the thalamus ends in the medial portion of the mediodorsal nucleus (MDm), a projection that exists in rats and monkeys (Krettek and Price, 1977; Porrino et al., 1981; Aggleton and Mishkin, 1984; Russchen et al., 1987) but is absent or negligible in cats and mice (Krettek and Price, 1977; Matyas et al., 2014). Importantly, the BLA projection to MDm originates from different neurons than those targeting the prefrontal or orbitofrontal cortex, with those innervating MDm having significantly larger somata (McDonald, 1987; Timbie and Barbas, 2015).

McDonald (1987) suggested that BLA cells projecting to MDm correspond to a specific subset of Golgi-defined class II neurons (McDonald, 1982), which generally correspond to GABAergic local-circuit cells. Consistent with this, studies using retrograde transport of tritiated aspartate found that BLA neurons innervating cortex (Carnes and Price, 1988) or striatum (Christie et al., 1987; Fuller et al., 1987) are labeled with this technique whereas those targeting MDm are not (Ray et al., 1992).

Yet, other lines of evidence indicate that BLA projections to MDm do not originate from GABAergic neurons. First, it was reported that BLA neurons contribute large axon terminals that form asymmetric synapses in MDm, similar to those provided by subcortical inputs to sensory thalamic nuclei (Kuroda and Price, 1991; Timbie et al., 2020). Second, most BLA axons projecting to MDm are immunoreactive for vesicular glutamate transporter 2 (VGLUT2) (Timbie and Barbas, 2015). However, since most MDm-projecting BLA neurons are located in its basolateral nucleus, and this nucleus is devoid of VGLUT2 expressing neurons (Hur and Zaborszky, 2005), these VGLUT2 axons might actually originate from a neighboring nucleus (Matyas et al., 2014).

Overall, the nature (excitatory vs. inhibitory) of the BLA projection to MDm remains unclear. Therefore, the present study aimed to shed light on this question using a combination of tract tracing, immunohistochemistry, optogenetics, and patch clamp recordings in rats.

MATERIALS AND METHODS

We performed two types of experiments. In the first, we aimed to identify what type of BLA cells project to MDm by combining retrograde tracing with immunohistochemistry. In the second, we studied the responses of MDm neurons to the optogenetic activation of BLA axons in brain slices in vitro.

Animals

We used Long-Evans rats of both sexes for all experiments (300-350 gm upon delivery; Charles River Laboratories, New Field, NJ; RRID: RGD_2308852). They had continuous access to water and food and were maintained on a 12-hour light-dark cycle (lights-off at 7:00 PM). All procedures were carried out during the light phase of the cycle, with the approval of the Institutional Animal Care and Use Committee of Rutgers University, and in compliance with the Guide for the Care and Use of Laboratory Animals (DHHS).

Surgical methods for tracer and virus infusions

Seven days or more after delivery, rats were deeply anesthetized with isoflurane, mounted in a stereotaxic apparatus, and administered atropine sulfate (0.05 mg/kg, i.m.) to aid breathing. Their scalp was cleaned with Betadine and alcohol. A local anesthetic (Bupivacaine, 0.125% solution, s.c.) was injected around the sites to be incised. Ten to fifteen minutes later, an incision was made on the scalp and a burr hole was drilled above the regions of interest (MDm for tracer infusions; BLA for virus infusions). Body temperature was kept at 37° C throughout the surgeries.

For the intra-cerebral infusions, we used glass pipettes pulled to an outer tip diameter of ~70 µm (PE-22, Narishige Instruments, Amityville, NY). Infusions proceeded at a rate of 9.6 nL/5 s using a

Nanoject II (Drummond Scientific Company, Broomall, PA). For retrograde labeling of BLA neurons projecting to MDm, we infused 150-200 nl of Fast Blue (FB; Polysciences, Warrington, PA) bilaterally into the MDm of 24 rats. For the optogenetic experiments, we infused one of the two following viruses: pAAV-hSyn-hChR2(H134R)-mCherry (Addgene, Watertown, MA # 26976-AAV5, 200 nl) or pAAV-mDlx-ChR2-mCherry-Fishell-3 (Addgene, # 83898-AAV9, 200 nl, 1:10) in the BLA of 39 and 30 rats, respectively.

Based on the stereotaxic atlas of Paxinos and Watson (2006), we used the following stereotaxic coordinates (in mm relative to bregma for the antero-posterior–AP, medio-lateral–ML, and dorso-ventral–DV axes): AP -2.4, ML 0.8, DV -5.0; AP -3.48, ML 0.6, DV -5.40 for MDm and AP -3.4, ML 5.1, DV -7.8 for the BLA. At the conclusion of the surgery, the wound was stitched with self-absorbing sutures, a local antibiotic was applied to the wound (Neosporin), and an analgesic was administered (Ketoprophen, 2 mg/kg, s.c., daily for 3 days).

Immunohistochemical procedures

Tissue preparation. Two weeks after the tracer infusions, rats were deeply anesthetized with isoflurane and perfused through the heart with 200 ml of 0.1 M phosphate buffer solution (PB, pH 7.4; 4°C) followed by 200 ml of a fixative containing 4% paraformadehyde in 0.1 M PB at 4°C. The brain was then extracted from the skull, post-fixed in the same fixative overnight, transferred to a 30% glucose solution until it sank, at which point it was sectioned with a freezing microtome at a thickness of 60 µm. One section out of four was set aside for counterstaining with cresyl violet. Sections were placed in PBS (0.01 M; pH 7.4) until further processing.

Selection of GABAergic markers. The BLA contains a similar variety of GABAergic neurons as found in the cerebral cortex (McDonald and Betette, 2001; McDonald and Mascagni, 2001a,b, 2002;

Mascagni and McDonald, 2003; Mascagni and McDonald, 2007; Vereczki et al., 2021). In descending order of numerical importance, the main subtypes are: cells expressing (1) parvalbumin (PV^+; ~43%), (2) somatostatin (SOM^+; ~18%), (3) cholecystokinin (CCK^+; ~15%), or (4) 5-HT-3A receptors (~7%). These peptides often colocalize with others. For instance, there are two main subtypes of CCK^+ cells: small CCK^+ cells that also express vasoactive intestinal peptide (VIP^+), and large multipolar ones that do not. Similarly, a proportion of SOM^+ cells also express nitric oxide synthase (NOS^+; Vereczki et al., 2021). However, co-localization with calcium-binding proteins is particularly prevalent. For instance, calbindin (CB; ~50%) is expressed by ~80% of PV^+ cells, ~90% of SOM^+ cells, and a low proportion of large CCK^+ cells (McDonald and Betette, 2001; McDonald and Mascagni, 2002). By contrast, calretinin (CR; ~20%) is expressed by many VIP^+ and small CCK^+ neurons (McDonald and Mascagni 2001a, 2002; Mascagni and McDonald 2003). Since we aimed to determine whether some MDm-projecting BLA neurons are GABAergic, we examined whether BLA neurons retrogradely labeled with FB also expressed various markers of GABAergic interneurons, which together are present in the vast majority of BLA interneurons: PV, CB, SOM, CR, NOS, CCK.

Immunohistochemical protocol. Sections were incubated overnight at room temperature with one of the primary antibodies listed in **Table 1**. These antibodies have been thoroughly characterized in previous studies on the amygdala, cortex, or related systems (PV: Trouche et al., 2019; Katona et al., 2020; Pesarico et al., 2022; CB: Larsson, 2018; Jablonski et al., 2021; SOM: Moga et al., 1989; Dabrowska and Rainnie, 2010; Suzuki and Bekkers, 2010; CR: Zhang et al., 2017; NOS: Clancy et al., 2001; Pla et al. 2006; Carrillo et al., 2007; Day-Brown et al., 2017; CCK: Whissell et al., 2015; Oláh et al., 2020; Poleksic et al., 2021). The pattern of labeling we obtained with each antibody conformed with prior descriptions (McDonald, 1989; McDonald and Mascagni, 2001, 2002, 2007; Mascagni and

McDonald, 2003). Moreover, omitting the primary antibody from the incubations resulted in a complete lack of differentiated labeling.

The primary antibody solutions also contained 0.3% Triton-X, 1% normal goat serum, and 0.02% sodium azide in PBS (0.01 M; pH 7.4). Sections were incubated in the primary antibody solution overnight. Then, after rinsing three times in PBS (0.01 M; pH 7.4) for 10 mins, the sections were incubated at room temperature with one of the corresponding secondary antibodies listed in **Table 1** for two hours. The secondary antibody solution also contained 0.3% Triton-X, 1% normal goat serum, and 0.02% sodium azide in PBS (0.01 M; pH 7.4). The sections were then washed repeatedly in PBS (0.01 M; pH 7.4) and mounted onto gelatine-coated slides. Finally, Prolong Gold anti-fade reagent (Invitrogen, Carlsbad, CA) was applied to the sections before covering them with a glass coverslip.

Criteria used for the identification of immunopositive neurons and search for double-labeled neurons. To minimize the incidence of false positives, a neuron was only considered immunoreactive for a given interneuronal marker if its entire soma, not only its periphery, displayed a level of immunostaining distinctly above background and similar to that seen in the most intensely labeled cells in the field of view. Also, since some interneuron subtypes are not homogeneously distributed in the BLA, we only assessed whether a cell labeled with FB also expressed an interneuronal marker if there were immunopositive neurons near the cell in question.

Electrophysiological experiments

Slice preparation. In vitro optogenetic experiments were conducted six to eight weeks after the virus infusions to ensure sufficient expression of the transgenes. Rats were deeply anesthetized with isoflurane until reflexes disappeared and then perfused through the heart with an ice-cold solution containing (in mM): 103 N-Methyl-D-glucamine, 2.5 KCl, 10 $MgSO_4$, 30 $NaHCO_3$, 1.2 NaH_2PO_4, 0.5

198 $CaCl_2$, 25 glucose, 20 N-2-hydroxyethylpiperazine-N′-2-ethanesulfonic acid (HEPES), 2 thiourea, 3 Na-
199 pyruvate, and 12 N-acetyl-L-cysteine. The brains were then extracted from the skull and sectioned (300
200 µm) in the coronal plane using a vibrating microtome while immersed in the above solution. Slices were
201 then kept in an oxygenated solution containing (in mM): 126 NaCl, 2.5 KCl, 1 $MgCl_2$, 26 $NaHCO_3$, 1.25
202 NaH_2PO_4, 2 $CaCl_2$, and 10 glucose (pH 7.3, 300 mOsm) at 34°C for 5 min and returned to room
203 temperature. At least one hour later, individual slices were transferred to the recording chamber, which
204 was perfused (6 ml/min) with the same solution (32°C).

205 *Electrophysiology.* Using infrared differential interference contrast microscopy, we obtained
206 whole-cell recordings of neurons in MDm. Recording pipettes were pulled from borosilicate glass
207 capillaries (resistance 5-8 MΩ) and filled with a solution containing (in mM): 130 K-gluconate, 10
208 HEPES, 10 KCl, 2 $MgCl_2$, 2 ATP-Mg, and 0.2 GTP-tris(hydroxymethyl)aminomethane, pH 7.2 (280
209 mOsm). Membrane potential (V_m) values were not corrected for the junction potential (10 mV with this
210 solution). MDm neurons were recorded in current-clamp mode with a MultiClamp 700B Amplifier
211 (Molecular Devices, San Jose, CA). The data was digitized at 20 kHz with a Digidata-1550 interface
212 controlled by pClamp-10.3 (Molecular Devices, San Jose, CA).

213 To activate ChR2-expressing BLA axons in MDm, we applied blue light stimuli (2 ms) at 0.2, 4,
214 8, 20, and 50 Hz using a blue LED (Mightex, Ontario, Canada) coupled to the light path. Postsynaptic
215 potentials were evoked from different membrane potentials (V_ms), as determined by current injection. To
216 study the electroresponsive properties of recorded cells, current pulses increasing in steps of ±20 pA (500
217 ms; 0.2 Hz) were applied from rest and other V_ms, as determined by current injection.
218
219 **Drugs**

As detailed in the Results section, one or more of the following drugs were added to the perfusate to identify the neurotransmitter and receptors involved in mediating light-evoked responses: DL-2-amino-5-phosphonopentanoic acid (AP5, 100 μM) to block NMDA receptors, 6-Cyano-7-nitroquinoxaline-2,3-dione disodium salt (CNQX, 10 μM) to block AMPA receptors, picrotoxin (100 μM) to interfere with GABA-A responses, (3-Aminopropyl)(diethoxymethyl)phosphinic acid (CGP35348, 10 μM) to block GABA-B responses, tetrodotoxin (TTX; 1 μM) to block voltage-gated Na^+ channels, and 4-aminopyridine (4-AP; 100 μM) to block K^+ channels involved in repolarization following action potentials. These drugs were obtained from Sigma (St. Louis, MO).

Statistical analyses

Analyses were performed with Clampfit 10.3 (Molecular Devices, San Jose, CA), off-line. All values are expressed as means ± SEM. We only considered cells that had a stable resting potential and generated overshooting action potentials. No data was excluded. All statistical tests are two-sided. We adopted a significance threshold of $p = 0.05$ for all statistical tests. We used Fisher Exact tests to compare the incidence of particular properties in different samples. Rank Sum tests were used to assess the significance of differences between two independent samples. Signed-rank tests were used to assess the significance of differences between two related samples. We also ran non-parametric ANOVAs (Friedman test) when comparing three matched samples of MDm neurons. To minimize subjective bias in the data analysis, we adopted a standard criterion for the identification of response onsets (voltage deviations > twice the noise, which then increased in amplitude without returning to baseline until the end of the response).

Data and code accessibility

The full dataset has not been deposited in a public repository because of its size but is available from the corresponding author upon request.

RESULTS

Retrograde labeling found in the amygdala following FB injections in MDm

A total of 24 rats received bilateral infusions of the retrograde tracer FB in MDm. The data described below was obtained in a subset of 15 rats in which the FB injections were centered on MDm bilaterally (see **Fig. 1A** for a representative example). In most experiments, FB diffused into one or more neighboring thalamic nuclei like the habenula, central lateral, paracentral, paraventricular, or central medial thalamic nuclei. However, since these sites are devoid of inputs from the BLA (Krettek and Price, 1977; Pitkanen et al., 2000), this tracer diffusion could not have resulted in the retrograde labeling we observed in the BLA.

Figure 1B plots the distribution of retrogradely labeled amygdala cells in a representative case. Consistent with prior descriptions in rats (McDonald, 1987) and monkeys (Aggleton and Mishkin, 1984; Russchen et al., 1987), FB^+ cells were not only observed in the BLA, but also in the medial, central, and cortical amygdala nuclei as well as several adjacent structures like the amygdalohippocampal area, endopiriform nucleus, and claustrum (**Fig. 1B**). In the BLA, retrogradely labeled cells were most concentrated in its caudal two thirds (**Fig. 1B**). They were present in all three components of the BLA (lateral, basolateral, and basomedial nuclei; **Fig. 1B**) and often occurred in conspicuous clusters of 4-12 closely spaced neurons (**Fig. 1C**). Even within such clusters, FB-labeled BLA neurons had heterogeneous morphological properties, including pyramidal, stellate, and spindle-shaped neurons of up to 50 μm in their long axis (**Fig. 1C**).

Expression of interneuronal markers among MDm-projecting BLA neurons

We aimed to determine whether some MDm-projecting BLA neurons are GABAergic. However, prior studies reported that in many GABAergic projection neurons, somatic levels of GABA are too low for immunohistochemical detection (Tóth and Freund, 1992). Thus, to minimize the likelihood of false negatives, we examined whether BLA neurons retrogradely labeled with FB also expressed various markers of BLA interneurons, which together should label the vast majority of BLA interneurons (see Methods). For each GABAergic marker, we assessed co-localization with FB in 7 to 15 sections from 2 to 7 different animals. See details in **Table 2**.

We first examined whether FB^+ BLA cells are immunoreactive for the Ca^{2+}-binding proteins CB and CR, since these two types of interneurons account for a large proportion (~70%) of GABAergic cells in the BLA (Mascagni and McDonald, 2007). As shown in the representative examples of **figure 2A**, not a single instance of CB-expressing FB^+ cell was observed. Consistent with the fact that a high proportion (~90%) of cells expressing PV are also immunoreactive for CB (McDonald and Betette, 2001), no FB^+ cells expressed PV (**Fig. 2B**). Surprisingly however, although many SOM^+ cells are known to also express CB (McDonald and Mascagni, 2002), a substantial proportion of FB^+ cells (21.7 ± 4.3%; 12 sections from 4 rats) were immunopositive for SOM (**Fig. 2C**). Since a proportion of BLA SOM^+ cells express NOS (Vereczki et al., 2021) and some cortical NOS^+ neurons contribute long-range projections (Tomioka et al., 2005; Christenson et al., 2019), we next assessed whether FB^+ cells express NOS. However, no instance of FB-NOS co-localization was observed (**Fig. 2D**). As to CR, a low proportion of FB^+ cells (10.9 ± 2.3%; 7 sections from 3 rats) were immunoreactive for this Ca^{2+}-binding protein (**Fig. 3A,B**). Since CR is expressed by many small CCK^+ neurons (Mascagni and McDonald, 2003), we also tested whether FB^+ cells expressed CCK. However none of them did (**Fig. 3C,D**).

Responses of MDm neurons to optogenetic activation of BLA axons

The above findings suggest that the BLA sends a mixed GABAergic-glutamatergic projection to MDm. Seeking independent corroboration for these results, we examined the responses of MDm neurons to optogenetic activation of BLA axons using visually guided whole-cell recordings *in vitro*. Thus, six to eight weeks prior to the electrophysiological experiments, rats received infusions of pAAV-hSyn-hChR2(H134R)-mCherry or pAAV-mDlx-ChR2-mCherry-Fishell-3, viruses that drive expression of channelrhodopsin (ChR2) under the control of a synapsin promoter or a Dlx enhancer, respectively. For simplicity, we hereafter refer to rats infused with these viruses as "Synapsin rats" (n=39) or "Dlx rats" (n=30), respectively. The data described below was obtained in a subset of these rats (23 and 12, respectively) where robust mCherry expression was observed in the BLA and no infected somata were detected outside the BLA (**Fig. 4A1, A2**).

While a synapsin promoter drives transgene expression in glutamatergic and GABAergic neurons (Kugler et al., 2003), the Dlx enhancer is expected to do so preferentially (if not selectively) in GABAergic cells (Dimidschstein et al., 2016). Yet, the two viruses gave rise to anterograde labeling of similar intensity in MDm (**Fig. 4B1, B2**). Moreover, as detailed in **Table 3**, optogenetic activation of BLA axons with the two viruses elicited a similar response pattern in MDm neurons, including a similar proportion of evoked EPSPs. This unexpected observation suggests that while the Dlx enhancer may favor transgene expression in GABAergic cells (Dimidschstein et al., 2016), it does not prevent their expression in glutamatergic neurons. Since the results obtained in the two sets of animals were very similar, they are pooled together below.

We tested the impact of optogenetically activating BLA inputs in 177 MDm neurons that generated overshooting action potentials and had stable resting potentials negative to -60 mV. The electroresponsive properties of recorded cells matched earlier descriptions of thalamocortical neurons (Jahnsen and Llinas, 1984a,b). That is, they displayed two firing modes depending on their V_m: tonic

314 firing when depolarized from positive to ~ –60 mV and a bursting firing pattern when depolarized from
315 more negative V_ms (**Fig. 5A**). Moreover, they generated rebound high-frequency spike bursts shortly after
316 the end of hyperpolarizing current pulses (**Fig. 5B**).

317 Blue light stimuli (2 ms) were applied in a wide range of frequencies (0.2-50 Hz). When light
318 stimuli evoked a synaptic response, the cells' V_m was set to different values (-55 mV to -100 mV) by
319 current injection to distinguish EPSPs from IPSPs. Qualitatively identical results were obtained in male
320 and female rats (**Table 4**). Optogenetic activation of BLA axons elicited synaptic responses in 21% or 37
321 of 177 MDm neurons (**Figs. 6-8**). In descending order of incidence, response types included an EPSP only
322 (73% or 27 of 37 of responsive cells; latency of 3.84 ± 0.35 ms; **Figs. 6,7**), an isolated IPSP (16% or 6 of
323 37 responsive cells; latency of 4.61 ± 1.37 ms; **Fig. 8B,D**), or an EPSP overlapping with an IPSP (11% or
324 4 of 37 responsive cells; **Fig. 8A,C**). The latency of EPSPs and isolated IPSPs did not differ significantly
325 (Rank Sum test, $p = 0.79$).

326 Properties of EPSPs elicited in MDm neurons by the optogenetic excitation of BLA axons. Light-
327 evoked EPSPs persisted after addition of TTX (1 μM) and 4-AP (100 μM) to the perfusate (**Fig. 6A**; six
328 tested cells), indicating that they were monosynaptic. Moreover, they were abolished or largely reduced
329 by addition of the AMPA and NMDA receptor antagonists CNQX (10 μM) and AP5 (100 μM) to the
330 perfusate (**Fig. 6A,B**; seven tested cells). When measured at the resting potential, light-evoked EPSPs had
331 a 20 to 80% risetime of 5.27 ± 0.82 ms (n=31) and a low amplitude (2.81 ± 0.44 mV; n=31). They never
332 elicited short-latency action potentials unless the cells were depolarized enough for the EPSP to reach
333 spike threshold (usually requiring depolarization to at least -60 mV; **Fig. 7A1**).

334 Presumably because light-evoked EPSPs interacted with the neurons' intrinsic voltage-dependent
335 conductances, their decay times (80 to 20% amplitude) varied markedly depending on the V_m from which
336 they were elicited (-85 mV, 39.3 ± 6.7 ms; -70 mV, 80.60 ± 12.3 ms; -55 mv, 110.52 ± 11.86 ms;

Friedman test, p=0.0002). For instance, in a subset of MDm cells (23%), light-evoked EPSPs had a characteristic "shoulder" when elicited from around -65 to -75 mV (that is in the bursting regime; **Fig. 7A2**), which was absent when cells were near spike threshold (**Fig. 7A1**) or hyperpolarized to around -85 mV and beyond (**Fig. 7A3**). The contrast is particularly striking in the inset of **figure 7A**, which shows a superimposition of light-evoked EPSPs elicited from different V_ms, but scaled to match their amplitude.

Light-evoked EPSPs showed a dependence on stimulation frequency, their amplitude dropping markedly when the stimulation frequency was increased (**Fig. 7B,C**). With an inter-stimulus interval (ISI) of 250 ms and 125 ms, the second EPSP's amplitude was 66.9 ± 9.8% (signed-rank test, p=0.005) and 63.5 ± 8.2 % (signed-rank test, p=0.002) of the first, respectively (**Fig. 7B)**. If the stimuli were applied in a range of Vm values where the first stimulus elicited a "shouldered" EPSP, the second EPSP's shoulder was also largely reduced or abolished (**Fig. 7C**).

Properties of IPSPs elicited by optogenetic excitation of BLA axons. Activation of BLA axons with blue light stimuli also elicited IPSPs, albeit in a significantly lower proportion of MDm cells (5.6%) than EPSPs (17.5%; Fisher exact test, p=0.0007). Although light-evoked IPSPs appeared to follow EPSPs in many cases (40% of cells with IPSPs; **Fig. 8A**), several factors suggest that these IPSPs were monosynaptic. First, the rat MDm does not contain local-circuit GABAergic cells (Jones, 2007). Second, when the IPSPs were blocked pharmacologically (n=3), the rising phase of EPSPs pre- vs. post-blockade diverged within ~1 ms of EPSP onset (**Fig. 8A**), the amplitude of the isolated EPSP becoming much higher than in control conditions (**Fig. 8A**). Third, in six MDm cells, blue light stimuli elicited IPSPs with no coincident EPSP (**Fig. 8B,D**). Fourth, in such cases, IPSP latencies (4.61 ± 1.37 ms; n=6) were nearly identical to EPSP latencies (3.84 ± 0.39 ms; n=27), inconsistent with a dependence of these IPSPs on the excitation of reticular thalamic neurons that project to MDm. Fifth, in these cells, light-evoked IPSPs

359 persisted after addition of CNQX (10 μM) and AP5 (100 μM) to the perfusate (**Fig. 8D1**; two of two
360 tested cells).

361 Light-evoked IPSPs had two components, an early picrotoxin-sensitive phase (100 μM; **Fig. 8B1**)
362 that reversed at, or slightly negative to, the resting potential (**Fig. 8B2, D2**) and is presumably mediated
363 by GABA-A receptors, and a late phase blocked by CGP35348 (10 μM) and therefore mediated by
364 GABA-B receptors (**Fig. 8B1**). In contrast with the EPSPs whose amplitude invariably dropped as the
365 stimulation frequency increased (**Fig. 7B,C**), light-evoked IPSPs were heterogeneous. Some showed little
366 attenuation during repetitive stimulation (**Fig. 8B3;** change from first to second IPSP: -13.27 ± 5.82 %
367 with 250 ms ISI; 8.09 ± 4.47% with 125 ms ISI; n=5). Others showed a marked attenuation with increased
368 stimulation frequency (**Fig. 8C**), revealing an underlying EPSP that was largely masked by the IPSP when
369 it was not attenuated (amplitude drop from first to second IPSP: 58.30 ± 9.69% with 250 ms ISI; 82.97 ±
370 13.88% with 125 ms ISI; n= 4).

DISCUSSION

The present study aimed to characterize BLA projections to MDm. The interest of this question stems from the fact that the medial prefrontal cortex, which is involved in higher order cognitive functions (Friedman and Robbins, 2021; Nett and LaLumiere, 2021), receives convergent inputs from MDm and BLA (Heidbreder and Groenewegen, 2003). Hence, projections from BLA to MDm could enhance the coordination of activity in this tripartite circuit.

Although many studies reported on BLA projections to MDm (Krettek and Price, 1977; Porrino et al., 1981; Aggleton and Mishkin, 1984; McDonald, 1987; Russchen et al., 1987), contradictory evidence has accumulated regarding the nature of this projection. It was initially suggested that it originates from long-range GABAergic cells (McDonald, 1987), a conclusion based on their distinctive morphology and the finding that they are not retrogradely labeled by deposits of tritiated aspartate in MDm (Ray et al., 1992), when the same technique labels BLA neurons that project to cortex (Carnes and Price, 1988) or striatum (Christie et al., 1987; Fuller et al., 1987).

However, subsequent studies cast doubt on this conclusion. First, it was found that the ultrastructural features of synapses formed by BLA axons with MDm neurons are similar to those of subcortical excitatory afferents ending in dorsal thalamic relay nuclei (Kuroda and Price, 1991; Timbie and Barbas, 2020). Moreover, BLA axons projecting to MDm were reported to be immunoreactive for VGLUT2, a marker of glutamatergic neurons (Timbie and Barbas, 2015). However, BLA neurons do not express VGLUT2 (Hur and Zaborszky, 2005), which led Matyas et al. (2014) to suggest that these VGLUT2 axons originate from the neighboring endopiriform nucleus.

Therefore, the present study was undertaken to determine whether BLA neurons projecting to MDm are GABAergic or glutamatergic. Overall, our results suggest that the BLA sends a mixed

393 projection to MDm, with a majority of the BLA neurons at the origin of this projection using glutamate as
394 a transmitter, and a minority, GABA.

395 *The BLA contains a small contingent of long-range GABAergic neurons that project to MDm*

396 In the present study, converging results from two different experimental approaches support the
397 conclusion that a proportion of MDm-projecting BLA neurons are long-range GABAergic cells. We first
398 tested whether BLA neurons retrogradely labeled by FB infusions in MDm were immunopositive for
399 various markers of GABAergic neurons. These analyses revealed that MDm-projecting BLA neurons do
400 not express CB, PV, NOS, or CCK. However, ~22% of them were immunopositive for SOM and ~11%
401 for CR. These findings are consistent with many prior studies that demonstrated the existence of long-
402 range GABAergic cells in a variety of systems (Caputi et al., 2013; Melzer and Monyer, 2020), including
403 the BLA (McDonald et al., 2012; McDonald and Zaric, 2015). Of note, while long-range GABAergic
404 cells are neurochemically heterogeneous (Caputi et al., 2013), several studies (Bakst et al., 1986; Jinno
405 and Kosaka, 2000; Tomioka et al., 2005, 2015; Melzer et al., 2012), including one on long-range
406 GABAergic cells of the BLA (McDonald and Zaric, 2015), reported that long-range GABAergic cells
407 express SOM, as found in the present study. By contrast, long-range CR neurons have been reported less
408 frequently and they accounted for a minority of long-range GABAergic cells (Toth and Freund, 1992;
409 Zappone and Sloviter, 2001; Tomioka et al., 2005).

410 In a second approach, we examined the responses of MDm cells to optogenetic activation of BLA
411 axons using visually guided whole-cell recordings *in vitro*. Consistent with the results of our
412 immunohistochemical experiments, optogenetic activation of BLA axons in MDm elicited mixed
413 glutamatergic-GABAergic responses or isolated GABAergic responses in 11% and 16% of responsive
414 cells, respectively. Since there are no local-circuit GABAergic neurons in the rat MDm (Jones, 2007), the
415 IPSPs could have resulted from the optogenetic activation of GABAergic axons arising in the BLA or

from the glutamatergic recruitment of reticular thalamic neurons that project to MDm. Inconsistent with the latter possibility however, the latency of light-evoked EPSPs and IPSPs was statistically indistinguishable. Moreover, addition of antagonists of ionotropic glutamate receptors did not abolish the IPSPs.

Impact of BLA inputs on MDm neurons

Together, our results indicate that the BLA contains glutamatergic and GABAergic neurons that project to MDm. *In vivo*, the impact of these neurons on MDm cells will depend on a variety of factors, many of which are at present uncharacterized. These factors include the number, strength, and location of the synapses along the somatodendritic axis of MDm neurons, the state of the recipient neurons (tonic vs. bursting regime), the dynamics of synaptic transmission (facilitating vs. depressing synapses), and the connections (if any) formed by glutamatergic and GABAergic BLA cells with each other or with different populations of BLA cells. We consider these various aspects in turn below.

Consistent with the fact that a minority of MDm-projecting BLA neurons expressed markers of GABAergic interneurons, light stimuli typically elicited EPSPs, alone or coinciding with IPSPs; light stimuli also occasionally elicited isolated IPSPs. Together, this data suggests that the BLA projection to MDm mainly originates from glutamatergic neurons, but that glutamatergic and GABAergic BLA cells often converge on the same MDm neurons. In our optogenetic experiments, even though light stimuli presumably caused a synchronous activation of most glutamatergic BLA axons to MDm, the EPSPs they elicited had a low amplitude and did not evoke spiking unless MDm neurons were depolarized beyond -60 mV by intracellular current injection. While the temporal overlap between light evoked EPSPs and IPSPs contributed to reduce EPSP amplitudes in some MDm cells, EPSPs continued to be of low amplitude after pharmacological abolition of GABA responses. Hence, when MDm cells are in the tonic

regime, glutamatergic BLA inputs cause a slight depolarization, which requires summation with other inputs or regenerative dendritic conductances to fire MDm cells. By contrast, when MDm cells are in the bursting regime, light-evoked EPSPs can elicit high-frequency spike bursts, likely because the depolarization they cause activates the low-threshold Ca^{2+} conductance.

Overall, the low amplitude of light evoked EPSPs suggests that glutamatergic BLA axons form few synapses with each target MDm neurons or that the efficacy of these synapses is low due to pre- or postsynaptic factors such as low release probability or receptor expression, respectively. Further reducing the impact of glutamatergic BLA axons onto MDm neurons is the dynamics of transmission at the synapses they form. That is, the amplitude of light-evoked EPSPs drops markedly when stimulation frequency is increased. Of note, it is unlikely that the low amplitude of light-evoked EPSPs resulted from a remote dendritic location of these synapses given prior electron microscopic studies indicating that BLA axon terminals are found on large dendritic shafts (Kuroda and Price, 1991; Timbie et al., 2020).

While light stimuli simultaneously activated glutamatergic and GABAergic BLA axons in our *in vitro* experiments, they may be recruited independently *in vivo*. For instance, the two types of MDm-projecting BLA cells may be driven by different inputs. Moreover, long-range GABA cells may form inhibitory synapses with MDm-projecting glutamatergic BLA cells. Finally, given precedents indicating that long-range GABAergic cells project to multiple sites (Jinno et al., 2007; Unal et al., 2018), we should not discount the possibility that the recruitment of MDm-projecting BLA cells is part of a large-scale coordination of activity at distributed sites.

REFERENCES

Aggleton JP, Mishkin M (1984) Projections of the amygdala to the thalamus in the cynomolgus monkey. *J Comp Neurol* **222**:56-68.

Alexander GE, DeLong MR, Strick PL (1986) Parallel organization of functionally segregated circuits linking basal ganglia and cortex. *Annu Rev Neurosci* **9**:357-81.

Bakst I, Avendano C, Morrison JH, Amaral DG (1986) An experimental analysis of the origins of somatostatin-like immunoreactivity in the dentate gyrus of the rat. *J Neurosci* **6**:1452-1462.

Carnes KM, Price JL (1988) Sources of presumptive glutamatergic/aspartergc afferents to the rat mesial prefrontal cortex. *Soc Neurosci Abstr* **14**:480.

Capogna M (2014) GABAergic cell type diversity in the basolateral amygdala. *Curr Opin Neurobiol* **26**: 110-6.

Caputi A, Melzer S, Michael M, Monyer H (2013) The long and short of GABAergic neurons. *Curr Opin Neurobiol* **23**:179-86.

Carrillo B, Pinos H, Guillamón A, Panzica G, Collado P (2007) Morphometrical and neurochemical changes in the anteroventral subdivision of the rat medial amygdala during estrous cycle. *Brain Res* **1150**:83-93.

Carlsen J, Heimer L (1988) The basolateral amygdaloid complex as a cortical-like structure. *Brain Res* **441**:377-380.

Christie MJ, Summers RJ, Stephenson JA, Cook CJ, Beart PM (1987) Excitatory amino acid projections to the nucleus accumbens septi in the rat: a retrograde transport study utilizing D[3H]aspartate and [3H]GABA. *Neuroscience* **22**:425-39.

Clancy B, Silva-Filho M, Friedlander MJ (2001) Structure and projections of white matter neurons in the postnatal rat visual cortex. *J Comp Neurol* 434:233-52.

Christenson Wick Z, Tetzlaff MR, Krook-Magnuson E (2019) Novel long-range inhibitory nNOS-expressing hippocampal cells. *Elife* **8**:e46816.

Dabrowska J, Rainnie DG (2010) Expression and distribution of Kv4 potassium channel subunits and potassium channel interacting proteins in subpopulations of interneurons in the basolateral amygdala. *Neuroscience* **171**:721-33.

Day-Brown JD, Slusarczyk AS, Zhou N, Quiggins R, Petry HM, Bickford ME (2017) Synaptic organization of striate cortex projections in the tree shrew: A comparison of the claustrum and dorsal thalamus. *J Comp Neurol* **525**:1403-1420.

Dimidschstein J et al. (2016) A viral strategy for targeting and manipulating interneurons across vertebrate species. *Nat Neurosci* **19**:1743-1749.

Friedman NP, Robbins TW (2022) The role of prefrontal cortex in cognitive control and executive function. *Neuropsychopharmacology* **47**:72-89.

Fuller TA, Russchen FT, Price JL (1987) Sources of presumptive glutamergic/aspartergic afferents to the rat ventral striatopallidal region. *J Comp Neurol* **258**: 317-38.

Groenewegen HJ, Berendse HW, Wolters JG, Lohman AH (1990) The anatomical relationship of the prefrontal cortex with the striatopallidal system, the thalamus and the amygdala: evidence for a parallel organization. *Prog Brain Res* **85**:95-116.

Heidbreder CA, Groenewegen HJ (2003) The medial prefrontal cortex in the rat: evidence for a dorso-ventral distinction based upon functional and anatomical characteristics. *Neurosci Biobehav Rev* **27**:555-79.

503 Hur EE, Zaborszky L (2005) Vglut2 afferents to the medial prefrontal and primary somatosensory
504 cortices: a combined retrograde tracing in situ hybridization study. *J Comp Neurol* **483**:351-73.
505 Jablonski J, Hoffmann L, Blümcke I, Fejtová A, Uebe S, Ekici AB, Gnatkovsky V, Kobow K (2021)
506 Experimental Epileptogenesis in a Cell Culture Model of Primary Neurons from Rat Brain: A
507 Temporal Multi-Scale Study. *Cells* **10**:3004.
508 Jahnsen H, Llinás R (1984a) Electrophysiological properties of guinea-pig thalamic neurones: an in vitro
509 study. *J Physiol* **349**:205-26.
510 Jahnsen H, Llinás R (1984b) Ionic basis for the electro-responsiveness and oscillatory properties of
511 guinea-pig thalamic neurones in vitro. *J Physiol* **349**:227-47.
512 Jinno S, Kosaka T (2000) Colocalization of parvalbumin and somatostatin-like immunoreactivity in the
513 mouse hippocampus: quantitative analysis with optical dissector. J Comp Neurol 2000, 428:377-388.
514 Jinno S, Klausberger T, Marton LF, Dalezios Y, Roberts JD, Fuentealba P, Bushong EA, Henze D,
515 Buzsáki G, Somogyi P (2007) Neuronal diversity in GABAergic long-range projections from the
516 hippocampus. *J Neurosci* **27**:8790-804.
517 Jones EG (2007) *The Thalamus*. Cambridge, Cambridge University Press.
518 Katona L, Hartwich K, Tomioka R, Somogyi J, Roberts JDB, Wagner K, Joshi A, Klausberger T,
519 Rockland KS, Somogyi P (2020) Synaptic organisation and behaviour-dependent activity of
520 mGluR8a-innervated GABAergic trilaminar cells projecting from the hippocampus to the subiculum.
521 *Brain Struct Funct* **225**:705-734.
522 Krettek JE, Price JL (1977) Projections from the amygdaloid complex to the cerebral cortex and thalamus
523 in the rat and cat. *J Comp Neurol* **172**: 687-722.
524 Kügler S, Kilic E, Bähr M (2003) Human synapsin 1 gene promoter confers highly neuron-specific long-
525 term transgene expression from an adenoviral vector in the adult rat brain depending on the
526 transduced area. *Gene Ther* **10**:337-47.
527 Kuroda M, Price JL (1991) Synaptic organization of projections from basal forebrain structures to the
528 mediodorsal thalamic nucleus of the rat. *J Comp Neurol* **303**:513-33.
529 Larsson M (2018) Non-canonical heterogeneous cellular distribution and co-localization of CaMKIIα and
530 CaMKIIβ in the spinal superficial dorsal horn. *Brain Struct Funct* **223**:1437-1457.
531 LeDoux JE, Farb C, Ruggiero DA (1990) Topographic organization of neurons in the acoustic thalamus
532 that project to the amygdala. *J Neurosci* **10**:1043-54.
533 Mascagni F, McDonald AJ (2003) Immunohistochemical characterization of cholecystokinin containing
534 neurons in the rat basolateral amygdala. *Brain Res* **976**:171-84.
535 Mascagni F, McDonald AJ (2007) A novel subpopulation of 5-HT type 3A receptor subunit
536 immunoreactive interneurons in the rat basolateral amygdala. *Neuroscience* **144**:1015-1024.
537 Mátyás F, Lee J, Shin HS, Acsády L (2014) The fear circuit of the mouse forebrain: connections between
538 the mediodorsal thalamus, frontal cortices and basolateral amygdala. *Eur J Neurosci* **39**:1810-23.
539 McDonald AJ (1982) Neurons of the lateral and basolateral amygdaloid nuclei: a Golgi study in the rat. *J*
540 *Comp Neurol* **212**:293-312.
541 McDonald AJ (1987) Organization of amygdaloid projections to the mediodorsal thalamus and prefrontal
542 cortex: a fluorescence retrograde transport study in the rat. *J Comp Neurol* 262:46-58.
543 McDonald AJ (1989) Coexistence of somatostatin with neuropeptide Y, but not with cholecystokinin or
544 vasoactive intestinal peptide, in neurons of the rat amygdala. *Brain Res* **500**:37-45.
545 McDonald AJ (1991) Organization of amygdaloid projections to the prefrontal cortex and associated
546 striatum in the rat. *Neuroscience* 44:1-14.

McDonald AJ (1992) Cell types and intrinsic connections of the amygdala. In: The Amygdala: Neurobiological Aspects of Emotion, Memory and Mental Dysfunction (Aggleton JP, ed), pp. 67-96. New York: Wiley Liss.

McDonald AJ, Betette RL (2001) Parvalbumin-containing neurons in the rat basolateral amygdala: morphology and co-localization of Calbindin-D(28k). *Neuroscience* **102**:413-25.

McDonald AJ, Mascagni F (2001a) Colocalization of calcium-binding proteins and GABA in neurons of the rat basolateral amygdala. *Neuroscience* **105**:681-93.

McDonald AJ, Mascagni F (2001b) Localization of the CB1 type cannabinoid receptor in the rat basolateral amygdala: high concentrations in a subpopulation of cholecystokinin-containing interneurons. *Neuroscience* **107**:641-52.

McDonald AJ, Mascagni F (2002) Immunohistochemical characterization of somatostatin containing interneurons in the rat basolateral amygdala. *Brain Res* **943**:237-44.

Mascagni F, McDonald AJ (2007) A novel subpopulation of 5-HT type 3A receptor subunit immunoreactive interneurons in the rat basolateral amygdala. *Neuroscience* **144**:1015-24.

McDonald AJ, Zaric V (2015) GABAergic somatostatin-immunoreactive neurons in the amygdala project to the entorhinal cortex. *Neuroscience* **290**:227-42.

McDonald AJ, Mascagni F, Zaric V (2012) Subpopulations of somatostatin-immunoreactive non-pyramidal neurons in the amygdala and adjacent external capsule project to the basal forebrain: evidence for the existence of GABAergic projection neurons in the cortical nuclei and basolateral nuclear complex. *Front Neural Circuits* **6**:46.

Melzer S, Michael M, Caputi A, Eliava M, Fuchs EC, Whittington MA, Monyer H (2012) Long-range-projecting GABAergic neurons modulate inhibition in hippocampus and entorhinal cortex. *Science* **335**:1506-1510.

Melzer S, Monyer H (2020) Diversity and function of corticopetal and corticofugal GABAergic projection neurons. *Nat Rev Neurosci* **21**:499-515.

Moga MM, Saper CB, Gray TS (1989) Bed nucleus of the stria terminalis: cytoarchitecture, immunohistochemistry, and projection to the parabrachial nucleus in the rat. *J Comp Neurol* **283**:315-32.

Nett KE, LaLumiere RT (2021) Infralimbic cortex functioning across motivated behaviors: Can the differences be reconciled? *Neurosci Biobehav Rev* **131**:704-721.

Oláh VJ, Lukacsovich D, Winterer J, Arszovszki A, Lőrincz A, Nusser Z, Földy C, Szabadics J (2020) Functional specification of CCK+ interneurons by alternative isoforms of Kv4.3 auxiliary subunits. *Elife* **9**:e58515.

Ottersen OP, Ben-Ari Y (1979) Afferent connections to the amygdaloid complex of the rat and cat. I. Projections from the thalamus. *J Comp Neurol* **187**:401-24.

Paxinos G, Watson C (2006) The Rat Brain in Stereotaxic Coordinates, 6th edition. San Diego, Academic Press.

Pesarico AP, Carceller H, Guirado R, Coviello S, Nacher J (2022) Long term effects of 24-h-restraint stress on the connectivity and structure of interneurons in the basolateral amygdala. *Prog Neuropsychopharmacol Biol Psychiatry* **115**:110512.

Pla R, Borrell V, Flames N, Marín O (2006) Layer acquisition by cortical GABAergic interneurons is independent of Reelin signaling. *J Neurosci* **26**:6924-34.

Pitkanen A (2000) Connectivity of the rat amygdaloid complex. In: The Amygdala: a functional analysis (Aggelton JP, ed), pp. 31-116. New York, Oxford University Press.

Poleksic J, Aksic M, Kapor S, Aleksic D, Stojkovic T, Radovic M, Djulejic V, Markovic B, Stamatakis A (2021) Effects of Maternal Deprivation on the Prefrontal Cortex of Male Rats: Cellular, Neurochemical, and Behavioral Outcomes. *Front Behav Neurosci* **15**:666547.

Porrino LJ, Crane AM, Goldman-Rakic PS (1981) Direct and indirect pathways from the amygdala to the frontal lobe in rhesus monkeys. *J Comp Neurol* **198**:121-36.

Ray JP, Russchen FT, Fuller TA, Price JL (1992) Sources of presumptive glutamatergic/aspartatergic afferents to the mediodorsal nucleus of the thalamus in the rat. *J Comp Neurol* **320**: 435-56.

Russchen FT, Amaral DG, Price JL (1987) The afferent input to the magnocellular division of the mediodorsal thalamic nucleus in the monkey, Macaca fascicularis. *J Comp Neurol* **256**: 175-210.

Smith Y, Paré D (1994) Intra-amygdaloid projections of the lateral nucleus in the cat: PHA-L anterograde labeling combined with postembedding GABA and glutamate immunocytochemistry. *J Comp Neurol* **342**: 232-248.

Spampanato J, Polepalli J, Sah P (2011) Interneurons in the basolateral amygdala. *Neuropharmacology* **60**:765-773.

Su HS, Bentivoglio M (1990) Thalamic midline cell populations projecting to the nucleus accumbens, amygdala, and hippocampus in the rat. *J Comp Neurol* **297**:582-93.

Suzuki N, Bekkers JM (2010) Inhibitory neurons in the anterior piriform cortex of the mouse: classification using molecular markers. *J Comp Neurol* **518**:1670-87.

Timbie C, Barbas H (2015) Pathways for Emotions: Specializations in the Amygdalar, Mediodorsal Thalamic, and Posterior Orbitofrontal Network. *J Neurosci* **35**:11976-87.

Timbie C, García-Cabezas MÁ, Zikopoulos B, Barbas H (2020) Organization of primate amygdalar-thalamic pathways for emotions. *PLoS Biol* **18**:e3000639.

Tomioka R, Okamoto K, Furuta T, Fujiyama F, Iwasato T, Yanagawa Y, Obata K, Kaneko T, Tamamaki N (2005) Demonstration of long-range GABAergic connections distributed throughout the mouse neocortex. *Eur J Neurosci* **21**:1587-600.

Tomioka R, Sakimura K, Yanagawa Y (2015) Corticofugal GABAergic projection neurons in the mouse frontal cortex. *Front Neuroanat* **9**:133.

Tóth K, Freund TF (1992) Calbindin D28k-containing nonpyramidal cells in the rat hippocampus: their immunoreactivity for GABA and projection to the medial septum. *Neuroscience* **49**:793-805.

Trouche S, Koren V, Doig NM, Ellender TJ, El-Gaby M, Lopes-Dos-Santos V, Reeve HM, Perestenko PV, Garas FN, Magill PJ, Sharott A, Dupret D (2019) A Hippocampus-Accumbens Tripartite Neuronal Motif Guides Appetitive Memory in Space**.** *Cell* **176**:1393-1406.e16.

Turner BH, Herkenham M (1991) Thalamoamygdaloid projections in the rat: a test of the amygdala's role in sensory processing. *J Comp Neurol* **313**:295-325.

Unal G, Crump MG, Viney TJ, Éltes T, Katona L, Klausberger T, Somogyi P (2018) Spatio-temporal specialization of GABAergic septo-hippocampal neurons for rhythmic network activity. *Brain Struct Funct* **223**:2409-2432.

Vereczki VK, Müller K, Krizsán É, Máté Z, Fekete Z, Rovira-Esteban L, Veres JM, Erdélyi F, Hájos N (2021) Total number and ratio of GABAergic neuron types in the mouse lateral and basal amygdala. *J Neurosci* **41**:4575-4595.

Vertes RP, Linley SB, Hoover WB (2015) Limbic circuitry of the midline thalamus. *Neurosci Biobehav Rev* **54**: 89-107.

Whissell PD, Cajanding JD, Fogel N, Kim JC (2015) Comparative density of CCK- and PV-GABA cells within the cortex and hippocampus. *Front Neuroanat* 9:124.

Zappone CA, Sloviter RS (2001) Commissurally projecting inhibitory interneurons of the rat hippocampal dentate gyrus: a colocalization study of neuronal markers and the retrograde tracer Fluoro-gold. *J Comp Neurol* 441:324-344.

Zhang T, Xu J, Maire P, Xu PX (2017) Six1 is essential for differentiation and patterning of the mammalian auditory sensory epithelium. *PLoS Genet* 13:e1006967.

TABLES

Primary Antibody	Source	Catalog #	Species	Concentration
Anti-parvalbumin	Synaptic Systems, Gottingen, Germany	24428	Guinea pig	1:1000
Anti-calbindin	Synaptic Systems, Gottingen, Germany	214004	Guinea pig	1:3000
Anti-calretinin	Invitrogen, Carlsbad, CA	MA5-14540	Rabbit	1:1000
Anti-somatostatin	ImmunoStar, Hudson, WI	20067	Rabbit	1:1000
Anti-nNOS	ImmunoStar, Hudson, WI	24287	Rabbit	1:1000
Anti-cholecystokinin	Sigma-Aldrich, St-Louis, MO	C2581	Rabbit	1:1000
Secondary Antibody				
Alexa Fluor-647 IgG	Invitrogen, Carlsbad, CA	A21450	Goat anti-guinea pig	1:500
Alexa Fluor 647 IgG	Invitrogen, Carlsbad, CA	A32733	Goat anti-rabbit	1:500

Table 1. Primary and secondary antibodies used in the present study. From left to right, columns indicate the name of the antibody, the company from which it was obtained, the catalog number, species, and concentration used.

	Calbindin	Parvalbumin	Somatostatin	Nitric oxide synthase	Calretinin	Cholecystokinin
Double-labeled FB^+ cells	0 %	0 %	21.7%	0 %	10.9%	0 %
FB^+ cells examined (n)	520	339	341	121	173	339
Cells positive for marker (n)	4021	2596	1128	152	807	680
Sections observed (n)	15	11	12	8	7	14
Rats (n)	2	3	4	3	3	7

Table 2. Proportion of MDm-projecting BLA cells (FB^+) that were immunoreactive for interneuronal markers. We only assessed whether FB^+ cells expressed an interneuronal marker when they were located within 200 µm of intensely immunoreactive neurons.

Promoter	Rats (n)	Tested Cells (n)	Responsive cells (%)	EPSP Incidence (%)	EPSP amplitude (average ± SEM)	IPSP Incidence (%)	IPSP amplitude (average ± SEM)
Synapsin	23	122	22.13	18.03	2.92 ± 0.55	4.10	1.83 ± 0.63
Dlx	12	55	18.18	16.36	2.56 ± 0.76	9.09	2.01 ± 1.07
			Fisher Exact test; p=0.69	Fisher Exact test; p=0.84	Rank Sum test; p=0.35	Fisher Exact test; p=0.29	Rank Sum test; p=0.30

Table 3. Comparison between optogenetic responses of MDm neurons in Synapsin and Dlx rats. The incidence of responsive cells, EPSPs, and IPSPs did not differ between the two promoters. Neither did the amplitude of EPSPs or IPSPs. EPSP amplitudes were measured at rest. IPSPs amplitudes were measured at -55 mV. Note that the in Dlx rats, the sum of the incidence of EPSPs and IPSPs is higher than the proportion of responsive cells because blue light stimuli elicited mixed (EPSP-IPSP) responses in some cells.

Sex	Rats (n)	Tested Cells (n)	Responsive cells (%)	EPSP Incidence (%)	EPSP amplitude (average ± SEM)	IPSP Incidence (%)	IPSP amplitude (average ± SEM)
Males	21	91	18.68	16.48	2.52 ± 0.34	4.40	2.22 ± 0.78
Females	14	86	23.26	18.6	3.08 ± 0.81	6.98	1.72 ± 0.90
			Fisher Exact test; p=0.27	Fisher Exact test; p=0.55	Rank Sum test; p=0.59	Fisher Exact test; p=0.52	NS

Table 4. Comparison between optogenetic responses of MDm neurons in male and female rats. The incidence of responsive cells, EPSPs, and IPSPs did not differ between the two groups of rats. Neither did the amplitude or EPSPs or IPSPs. EPSP amplitudes were measured at rest. IPSPs amplitudes were measured at -55 mV. Abbreviation: NS, not significant.

FIGURE LEGENDS

Figure 1. Fast Blue injection in MDm and resulting retrograde labeling in the amygdala. (**A1**) Bilateral FB infusion site in MDm. (**A2**) Cresyl violet-stained section, close to the one shown in **A1**. (**B**) Distribution of retrogradely labeled cells in the amygdala and immediately adjacent structures at three rostro-caudal levels (relative to bregma): (**B1**) -1.8 mm, (**B2**) -2.8 mm, (**B3**) -3.7 mm. In **B1-3**, each dot marks the location of a retrogradely labeled cell observed in a single 60 µm section. (**C**) Morphology of retrogradely labeled BLA neurons. Calibration bars in B3 and C4 apply to all panels of B and C, respectively. Abbreviations: AA, anterior amygdala area; AHA, amygdalohippocampal area; APir, amygdalopiriform transition area; ASt, amygdalostriatal transition area; BL, basolateral nucleus of the amygdala; BLP, posterior part of BL; BLV, ventral part of BL; BM, basomedial nucleus of the amygdala; cc, corpus callosum; CeC, CeM, and CeL, capsular, medial, and lateral sectors of the central nucleus of the amygdala; Cl, claustrum; CMT, central medial thalamic nucleus; Co, cortical nucleus of the amygdala; cp, cerebral peduncle; CPu, striatum; EGP, external part of the globus pallidus; EN, endopiriform nucleus; EP, entopeduncular nucleus; Hb, habenula; I, intercalated cell cluster; ic, internal capsule; IMD, intermediodorsal thalamic nucleus; LA, lateral nucleus of the amygdala; LP, lateral posterior thalamic nucleus; MDL, lateral part of the mediodorsal thalamic nucleus; MDm, medial part of the mediodorsal thalamic nucleus; ME, medial nucleus of the amygdala; opt, optic tract; Pir, piriform cortex; PMCo, posteromedial cortical amygdala; Po, posterior thalamic nuclear group; PVT, paraventricular thalamic nucleus; STIA, intra-amygdaloid division of the bed nucleus of the stria terminalis; LP, lateral posterior thalamic nucleus; V, ventricle; VM, ventromedial thalamic nucleus; VP, ventroposterior thalamic nucleus.

Figure 2. Immunoreactivity for calbindin, parvalbumin, somatostatin, and nitric oxide synthase among MDm-projecting BLA neurons. Each row shows (**1**) BLA neurons retrogradely labeled following Fast Blue infusions in MDm (pseudo-colored green); (**2**) Immunoreactivity for a particular interneuronal marker in the same BLA region (labels at bottom); (**3**) overlay of the previous two panels. (**A**) Calbindin (CB). (**B**) Parvalbumin (PV). (**C**) Somatostatin (SOM). (**D**) Nitric oxide synthase (NOS). **Filled arrows** point to double-labeled neurons. **Empty arrows** point to FB^+ neurons that are not immunoreactive for the interneuronal marker considered. Calibration bars in panel 1 of A-D, apply to all panels of A-D.

Figure 3. Immunoreactivity for calretinin and cholecystokinin among MDm-projecting BLA neurons. Each row shows (**1**) BLA neurons retrogradely labeled following FB infusions in MD (pseudo-colored green); (**2**) Immunoreactivity for a particular interneuronal marker in the same BLA region; (**3**) overlay of the previous two panels. (**A,B**) Calretinin (CR). (**C,D**) cholecystokinin (CCK). **Filled arrows** point to double-labeled neurons. **Empty arrows** point to FB^+ neurons that are not immunoreactive for the interneuronal marker considered. Calibration bars in panel 1 of A-D, apply to all panels of A-D.

Figure 4. Virus infusion sites in BLA and resulting labeling in MDm. (**A**) Examples of virus infusion sites with the synapsin promoter (**A1**) or Dlx enhancer (**A2**) and resulting labeling in MDm (**B1,2**). Calibration bar in A2 also applies to A1. Calibration bar in B1 also applies to B2. Abbreviations: ASt, amygdalo-striatal transition area; BL, basolateral nucleus of the amygdala; BM, basomedial nucleus of the amygdala; CeA, central nucleus of the amygdala; CMT, central medial thalamic nucleus; EC, external capsule; Hb, habenula; LA, lateral nucleus of the amygdala; MDL, lateral part of the mediodorsal thalamic

nucleus; MDm, medial part of the mediodorsal thalamic nucleus; ME, medial nucleus of the amygdala; Pir, piriform cortex; PVT, paraventricular thalamic nucleus.

Figure 5. Electroresponsive properties of MDm neurons. (**A,B**) Current-evoked responses in two representative MDm neurons recorded in Synapsin and Dlx rats, respectively. (**A**) Voltage response to depolarizing current pulses applied from a depolarized V_m (**A1**; -52 mV) or rest (**A2**; -70 mV). Typical of MDm neurons, this cell fires tonically from the depolarized level but generates high-frequency spike bursts from the more negative potential. **Inset**: high-frequency burst of action potentials depicted with a faster time base. (**B**) At the break of negative current pulses, MDm cell generates rebound high-frequency spike bursts. Time calibration in A1 also applies to A2. Voltage calibration in A2 also applies to A1.

Figure 6. Light-evoked EPSPs are monosynaptic and mediated by ionotropic glutamatergic receptors. (**A,B**) Light-evoked EPSPs in MDm neurons recorded in Dlx and Synapsin rats, respectively. Blue trace at bottom: light stimuli. (**A**) Superimposed light-evoked EPSPs in control conditions (top), after addition of TTX and 4-AP to the perfusate (middle), and further addition of CNQX (10 μM) and AP5 (100 μM; bottom, red). (**B**) Superimposed light-evoked EPSPs in control conditions (top, black), and after addition of CNQX and AP5 to the perfusate (bottom, red). In both panels, light stimuli were applied while recorded cells were at their resting potential.

Figure 7. Dependence of light-evoked EPSPs on membrane potential and stimulation frequency. (**A**) Response evoked by blue light stimuli when the MDm neuron was depolarized to -55 mV (**A1**; 6 trials), at rest (**A2**; 9 trials), or hyperpolarized to -85 mV (**A3**; 3 trials). In **A1,** suprathreshold (top) and subthreshold responses (bottom) are separated. **Inset in A1**: superimposition of light-evoked EPSPs elicited from different V_ms, but scaled to match their amplitude. (**B**) EPSPs evoked by blue light stimuli applied at different frequencies (0.2 Hz, top; 4 Hz, middle; 8 Hz, bottom). Stimuli were delivered at rest (-64 mV). (**C**) EPSPs evoked by blue light stimuli delivered at 4 Hz. Red trace at the top is the average of the five individual trials (black) shown below. Stimuli were delivered at rest (-70 mV). Same cell as in A.

Figure 8. Properties of light-evoked IPSPs. (**A-D**) Responses of four different MDm neurons to blue light stimuli delivered at 8 (A1,B3), 0.2 (B1,B2,D2), and 4 (C,D1) Hz. (**A**) MDm cell in which blue light stimuli elicited a mixed EPSP-IPSP response, before (black) and after (red) addition of picrotoxin (100 μM) and CGP35348 (10 μM) to the perfusate. Light stimuli (blue) were delivered at 8 Hz. The response to the first two stimuli in **A1** is shown with a faster time base in **A2**. (**B**) MDm cell in which blue light stimuli elicited pure IPSPs (black, Control). (**B1**) The late phase of the IPSP was sensitive to the GABA-B antagonist CGP35348 (10 μM; red, CGP) whereas its early phase was blocked by picrotoxin (black, CGP + Picro). (**B2**) Light evoked IPSPs at different V_ms (numbers on the left). (**B3**) Response of the same MDm neuron to trains of blue light stimuli at 8 Hz. Red trace at the top is the average of the five individual trials (black) shown below. (**C**) MDm cell in which light stimuli elicited a mixed EPSP-IPSP response. In this cell, IPSPs showed a marked attenuation with increased stimulation frequency. (**D1**) MDm cell in which light stimuli elicited pure IPSPs (black trace) that persisted after addition of CNQX and AP5 (red trace). (**D2**) Light evoked IPSPs at different V_ms in the same cell.

Figure 1

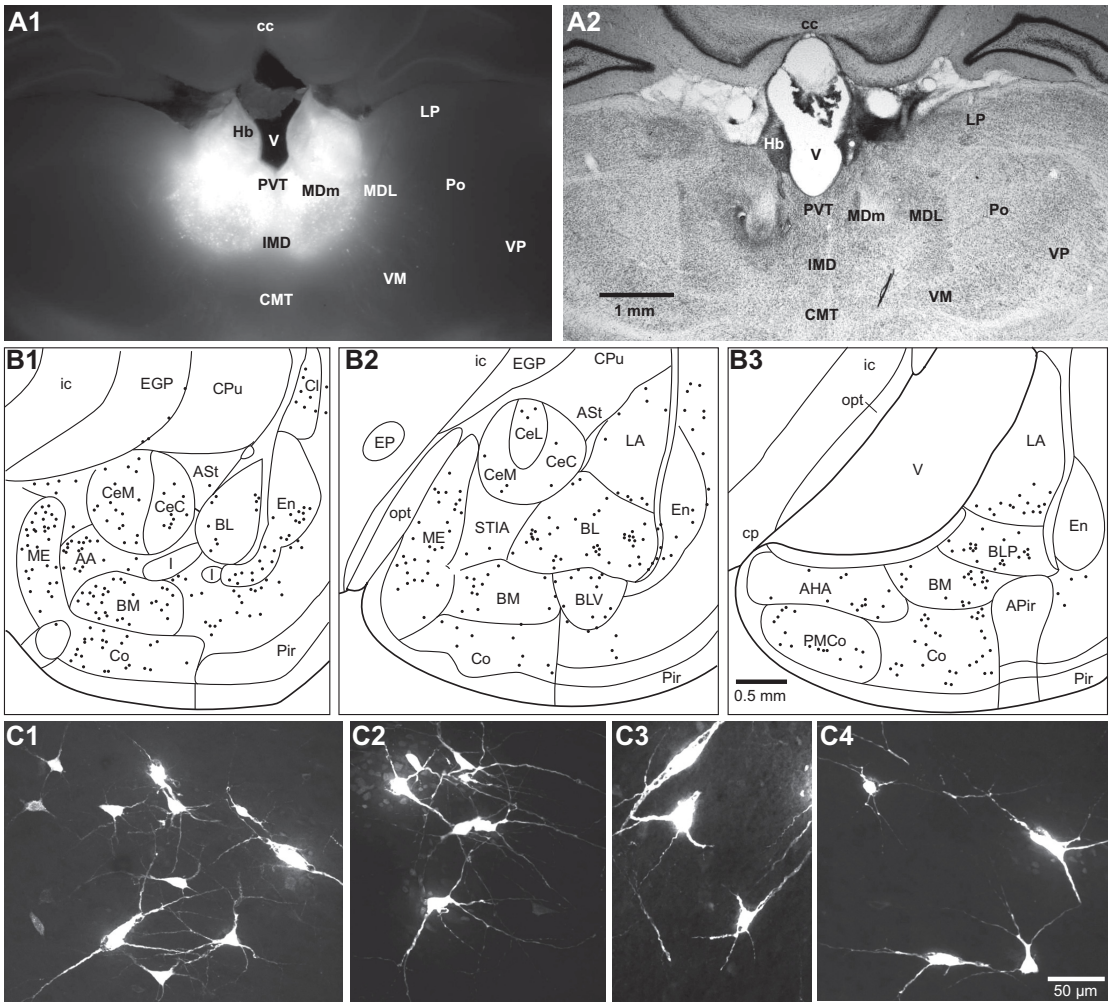

Figure 2

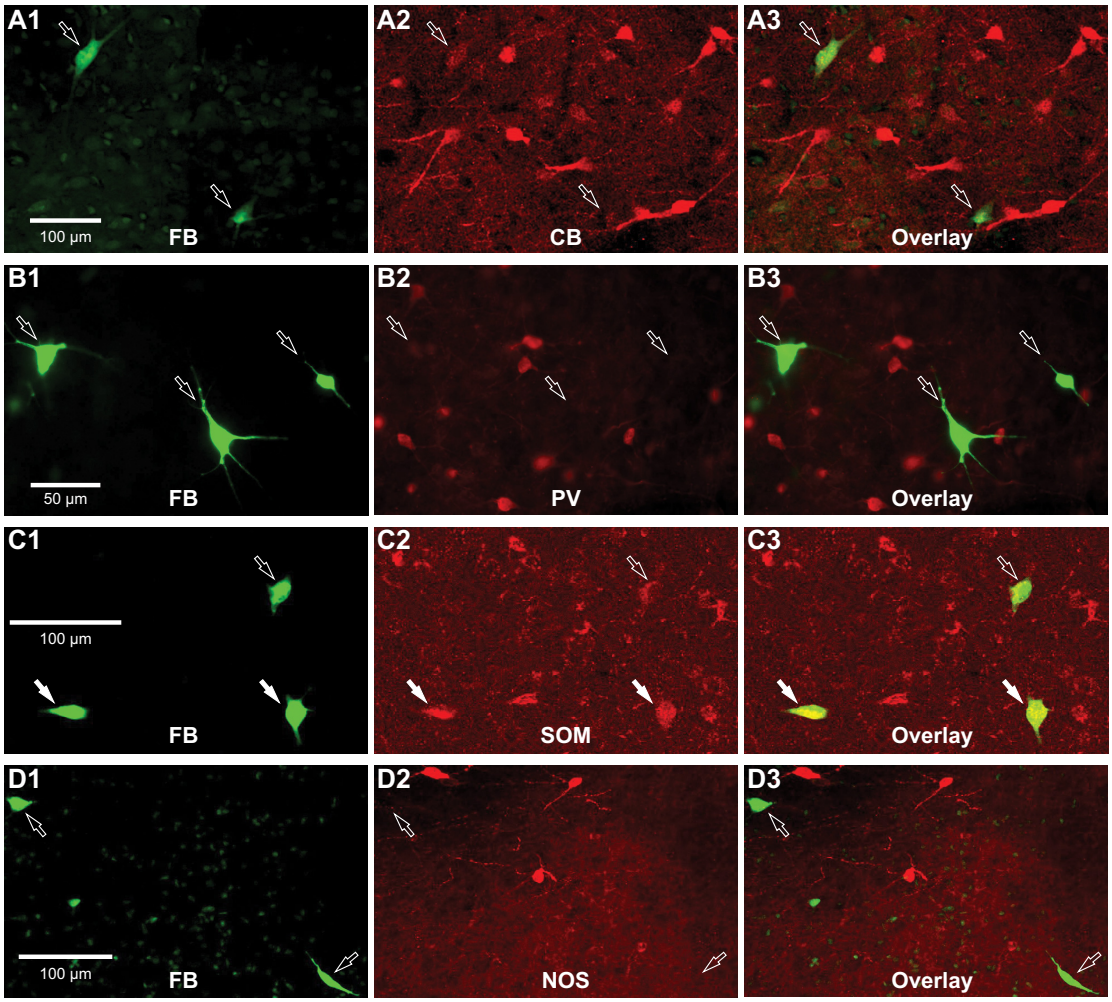

Figure 3

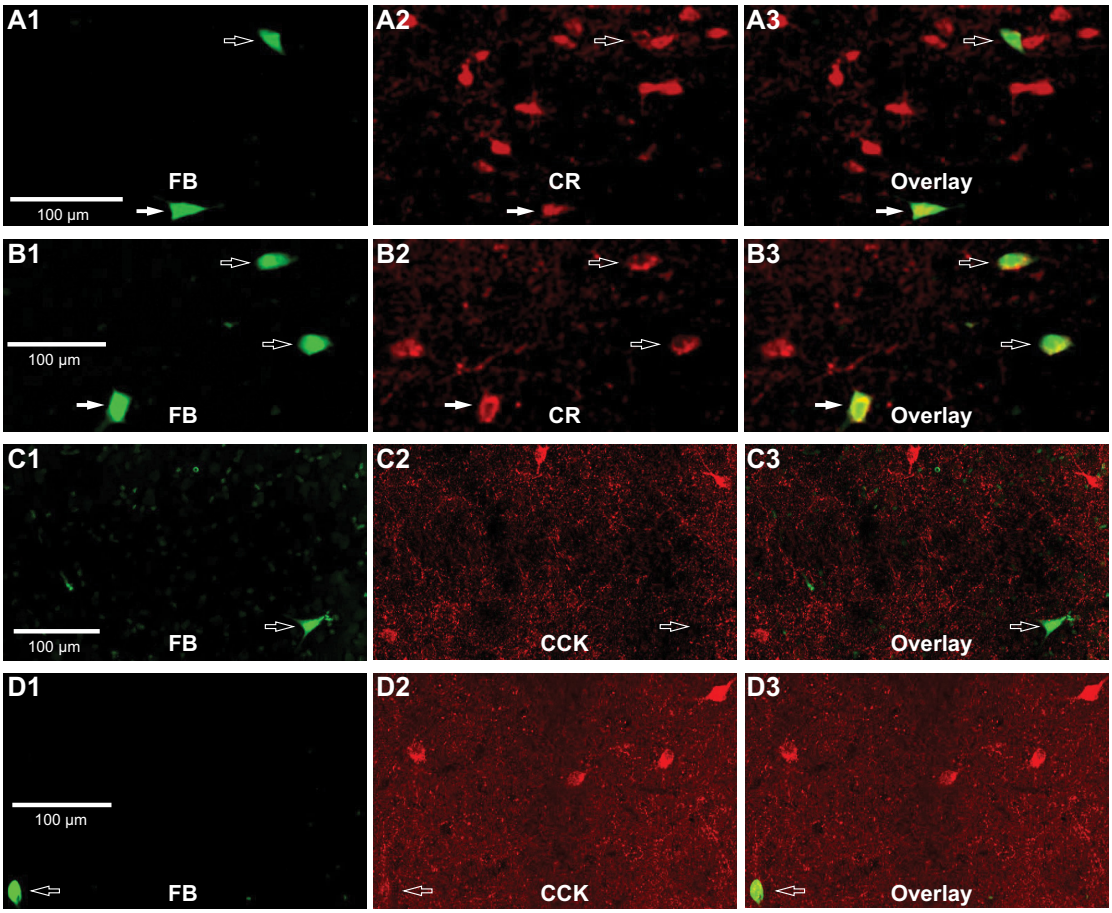

Figure 4

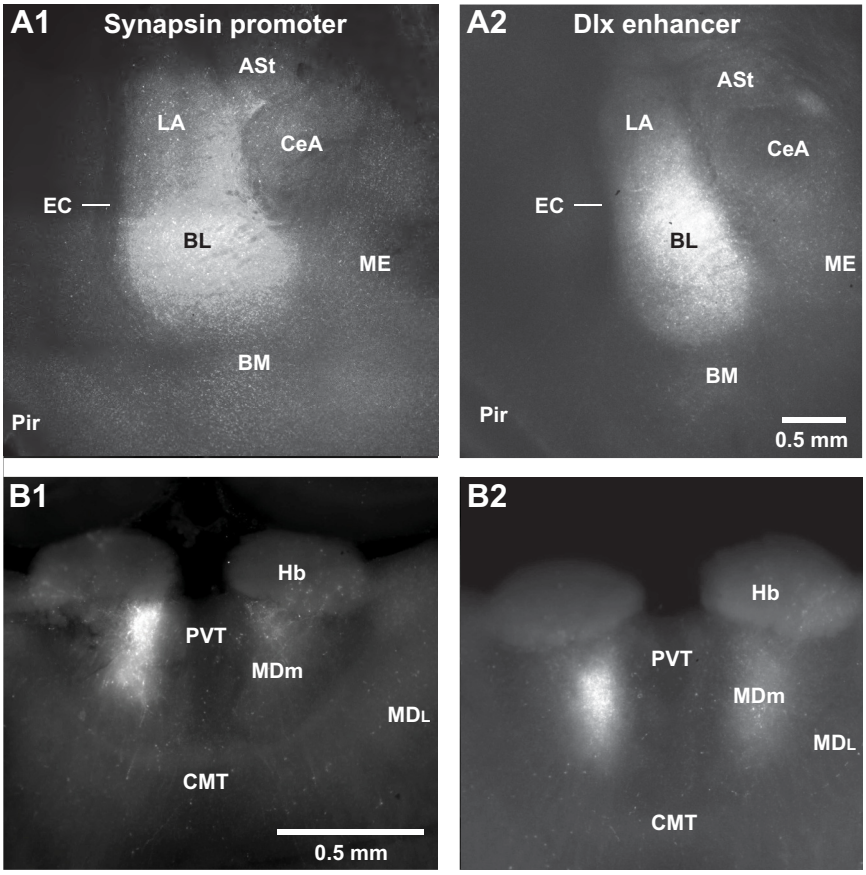

Figure 5

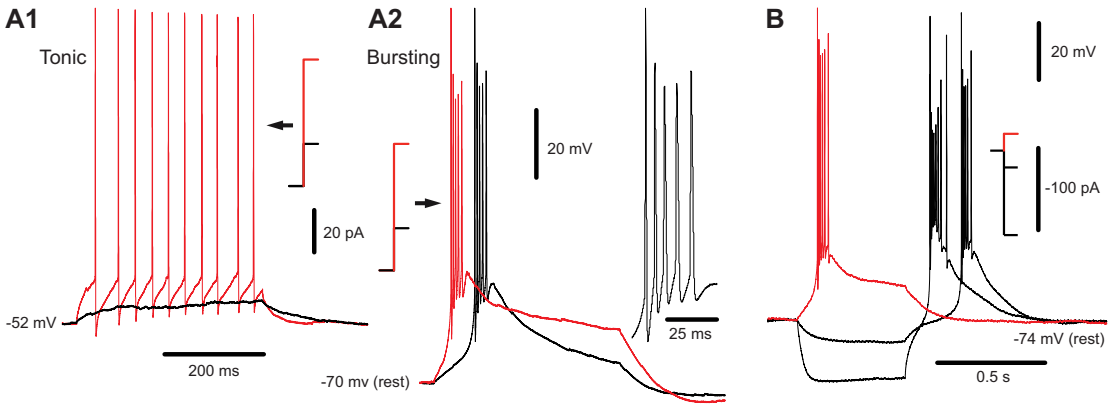

Figure 6

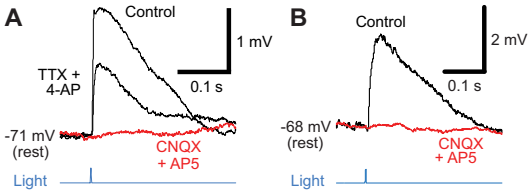

Figure 7